POAC'25
St. John's, Newfoundland and Labrador, Canada

Proceedings of the 28th International Conference on Port and Ocean Engineering under Arctic Conditions
Jul 13-17, 2025
St. John's, Newfoundland and Labrador
Canada

Exploring ice-induced vibrations on compliant conical structures with ice basin experiments

Alice Petry[1], Otto Puolakka[1], Arttu Polojärvi[1]

[1] Department of Energy and Mechanical Engineering, School of Engineering, Aalto University, Espoo, Finland

ABSTRACT

Offshore structures subjected to drifting level ice are often designed with ice cones or inclined structures at the waterline. Ice cones are known to reduce peak loads and sustained ice-induced vibrations from drifting sea ice. However, under certain ice drift conditions, compliant conical structures can still experience ice-induced vibrations due to repeated bending failure. This study explores a new method of studying ice-induced vibrations on compliant conical structures in an ice basin. The method combines a hardware-in-the-loop test setup, a numerical structure model of an offshore wind turbine, and a downward-breaking cone with a 60-degree slope angle. Each test was repeated with a cylindrical structure as a reference. The experiments resulted in different types of ice-induced vibrations on the cone, including bending failure-induced vibrations with lock-in characteristics and unexpected vibrations caused by local failure at the ice-structure interface with attributes of both shear and crushing failure. This paper presents a qualitative analysis of ice-induced vibrations on both structures.

KEY WORDS: ice cone, offshore wind turbine, structural dynamics, model ice

INTRODUCTION

Planned offshore wind farms in Arctic conditions, such as in the Northern Baltic Sea, need to be designed to sustain loads from yearly occurring sea ice. Offshore wind turbines (OWTs) are slender and compliant structures prone to ice-induced vibrations from drifting level ice (Hammer, Willems and Hendrikse, 2023). Common OWT substructures used in the Southern Baltic Sea, e.g., monopiles, may not withstand the expected ice loads (Van der Stap et al., 2023).

Ice cones are conical structures located at the ice-structure interaction point. These structures can reduce peak loads from drifting level ice because the sloped interface causes the ice to fail through bending failure instead of crushing failure. The presence of an ice cone also hinders the development of sustained ice-induced vibrations from drifting level ice, as observed on vertical structures. Kemi-I lighthouse is an example of a structure that ceased to experience continuous vibrations after the installation of an ice cone (Brown and Määttänen, 2009). Yue and Bi (1998, 2000) first reported ice-induced vibrations on a conical structure from the JZ20-

2 MUQ platform located in the Bohai Sea. The jacket structure was equipped with a double-sided ice cone, and it experienced dynamic amplification when the bending failure frequency of the ice matched a natural frequency of the structure.

To investigate ice-induced vibrations on compliant conical structures, researchers have performed model-scale ice basin experiments with rigid structure models connected to compliant support structures (Barker et al., 2005; Tian and Huang, 2013; Huang, Song and Shi, 2006; Huang, Ma and Tian 2013; Huang, Mu and Tian, 2013; Ziemer, Evers and Voosen, 2015). Each of these experiments used Cauchy-Froude scaling laws to scale the strength of the ice as well as the dynamic properties of the reference prototype structure. Only the experiments by Huang, Song and Shi (2006) and Tian and Huang (2013) observed bending failure-induced vibrations at model-scale. In these tests, the ice failed through a two-time bending failure process. First, the ice failed by bending into wedges. Second, these wedges failed again. The combined failure frequency excited a natural frequency of the structure and caused large structural oscillations. However, this two-time bending failure process is rarely reported in field observations, although it has been observed against steep structures (Xu et al., 2011; Kärnä and Jochmann, 2003).

Recent ice basin experiments (Petry et al., 2024) explored a new method of investigating ice-induced vibrations on compliant conical structures using a downward-breaking ice cone together with a novel hardware-in-the-loop (HiTL) system based on the hybrid technique (Hammer and Hendrikse, 2024) and a set of scaling laws focused on the preservation of kinematics of a reference structure (Hammer, Puolakka and Hendrikse, 2024), namely an OWT (Hammer, Willems and Hendrikse, 2023). During the experiments, the structure experienced bending failure lock-in and an unexpected regime of ice-induced vibrations caused by repeated local failure of the ice edge at the ice-structure interface at low ice drift speed. Petry et al. (2024) present a qualitative analysis of the different ice failure modes and the corresponding force (and displacement) signals on a rigid and a compliant ice cone at various ice drift speeds. The current paper compares the structural response of a compliant conical and a compliant cylindrical structure at low, medium and high ice drift speed, with a focus on ice-induced vibrations.

METHODS

Ice basin experiments were performed in April 2023 at the Aalto Ice and Wave Tank. The ice basin measures 40 m x 40 m in area and is 2.8 m deep. It is equipped with cooling technology to generate ethanol-doped granular model ice. Moreover, the ice basin is spanned by a bridge that holds a carriage. Both the bridge and the carriage can move across the ice basin.

Producing model ice followed the method outlined in (Li and Riska, 1996). First, the water-ethanol mixture was sprayed into the air at an ambient temperature of −10°C to create an initial ice-carrying layer. The spraying process continued until the ice reached the desired thickness of 25 mm. The ice then hardened overnight at an ambient temperature of −12°C. During the tests, the ambient temperature was −10°C. Maintaining this ambient temperature produced model ice with a high elastic modulus, flexural strength and compressive strength (Table 1) with favorable mechanical properties to study ice-induced vibrations on vertical structures (Hammer, Puolakka and Hendrikse, 2024). Although the mechanical properties varied significantly throughout the testing day, it is assumed that they remained constant over the duration of each test.

The tests were performed with a HiTL test setup (Figure 1) developed by Hammer and Hendrikse (2024). The HiTL setup consists of two aluminium plates that can move

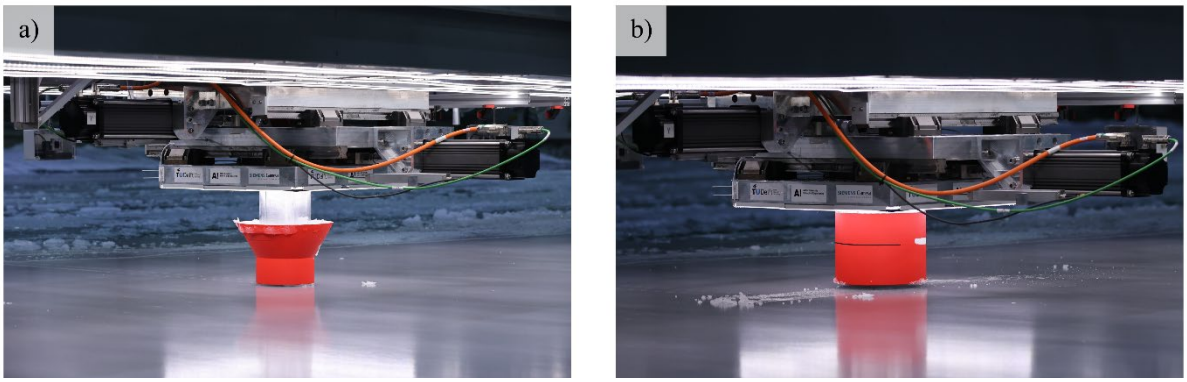

Figure 1. Overview of the HiTL test setup attached to the carriage at the Aalto Ice and Wave Tank: a) cone (reproduced from Petry et al., 2024), b) cylinder (reproduced from Hammer and Hendrikse, 2024).

perpendicular to each other using two integrated actuator motors. A cylindrical pile is connected to the bottom plate. This pile is instrumented with three flat load cells, which can measure the horizontal ice load on the pile or an attached structure model. Moreover, each aluminium plate is instrumented with a displacement sensor, which measures the position of the pile. The current experiments used a conical and a cylindrical structure model (Figure 1). The ice cone has a waterline diameter of 300 mm and a slope angle of 60 degrees. The cylinder also has a waterline diameter of 300 mm. The cylindrical section of the cone, which had a diameter of 225 mm, prevented ice fragments from passing below the cone. Both structures are made of selective laser-sintered polyamide 12. The test setup was considered rigid with an estimated global stiffness of 18 MN m^{-1} (Hammer, 2024). The stiffness of the combined carriage and test setup were not measured but are estimated to be similar.

A numerical structure model uploaded to a microcontroller controls the HiTL test setup. The numerical model takes the horizontal ice force (as measured) as an input and updates the position of the pile using a linearized lumped-mass model of a reference structure, a semi-implicit Euler-Cromer time-stepping algorithm, and a time-delay compensation algorithm (Hammer and Hendrikse, 2024). These algorithms form an open-loop control system. The current experiments used a structure model of an OWT with a monopile foundation located in the Southern Baltic Sea. Hammer, Willems, and Hendrikse (2023) describe the numerical OWT model in detail. Although the test setup and the numerical structure model moved in the ice-drift direction (Y) and perpendicular to it (side-to-side motion, (X)), the remaining paper focuses only on the ice-drift direction. The dynamic properties of the OWT in the ice-drift direction at the ice-structure interaction point are presented in Table 2.

The dynamic properties of the OWT model are scaled using a scaling factor λ defined as the ratio of the mean brittle crushing load on the reference OWT and on the model-scale structure (Hammer and Hendrikse, 2024). The resulting scaling factors were $\lambda = 1856$ for the conical structure and $\lambda = 1154$ for the cylindrical structure. In the case of the cone, this scaling factor should be interpreted as a sensitivity factor that enables ice-structure interaction at basin-scale.

The HiTL test setup is connected to the carriage via a bolted connection. During the experiments, the carriage moved the test setup through the ice at low (5 mm s^{-1}), medium (30 mm s^{-1}) and high (70 mm s^{-1}) speed. The carriage speed is referred to as the ice drift speed v_i, because this setup imitates ice drifting against a stationary structure.

Table 1. Mechanical properties of the model ice. The target ice thickness was 25 mm. The measured ice thickness varied between 27 mm and 37 mm.

Testing time	Elastic modulus [MPa]	Flexural strength [kPa]	Compressive strength [kPa]	Compressive-to-flexural-strength-ratio
~ 9:00	2581	464	759	1.6
~ 18:00	5012	545	1054	1.9

Table 2. Dynamic properties for the lumped mass model of an OWT at the ice-structure interaction point (mean sea level, MSL). The dynamic properties were scaled with a scaling factor $\lambda = 1856$ for the conical structure and $\lambda = 1154$ for the cylindrical structure. Only the properties in the ice-drift direction are provided.

Mode [#]	Natural frequency [Hz]	Critical damping coefficient [%]	Mode-shape amplitude at MSL – cone [10^{-3} kg$^{-0.5}$]	Mode-shape amplitude at MSL – cylinder [10^{-3} kg$^{-0.5}$]
1	0.153	0.8	-1.94	-1.529
2	0.824	1.2	13.23	10.43
3	1.504	2.6	20.16	15.89
4	2.722	5.4	9.92	7.822
5	5.110	5.4	-9.81	-7.734
6	7.458	5.4	19.44	15.32
7	10.47	5.4	-2.46	-1.936
8	13.39	5.4	-16.84	-13.28
9	15.27	5.4	6.42	5.058
10	17.26	5.4	-9.58	-7.552

RESULTS

Low ice drift speed (5 mm s^{-1})

Figure 2 presents the force-time and displacement-time signals and their corresponding amplitude spectral densities (ASDs) at a low ice drift speed (v_i = 5 mm s^{-1}). Both the force-time and the displacement-time signals are composed of sawtooth waves on top of an increasing mean. Each sharp force drop represents the local failure of the ice edge at the ice-cone interface. Each local failure event unloaded the cone momentarily, allowing the cone to move towards the ice edge (against the ice-drift direction). The ASD of the displacement signal indicates that the cone was experiencing oscillations at a frequency just below its second natural frequency (f_n). The amplitude of these oscillations was small (about 3 mm to 4 mm). The ASD of the force signal is less straightforward to interpret as it shows multiple peaks with similar amplitudes at different frequencies. Nonetheless, the force-time signal shows load drops at regular intervals with a failure frequency of around 1 Hz to 2 Hz.

In contrast, the force-time and displacement-time signals on the cylinder are characteristic of intermittent brittle crushing. Both signals are composed of sawtooth waves. The first natural frequency is the dominant frequency in both the force and displacement ASDs. Note that the amplitudes of the force and displacement signals are significantly more prominent on the cylinder than on the cone.

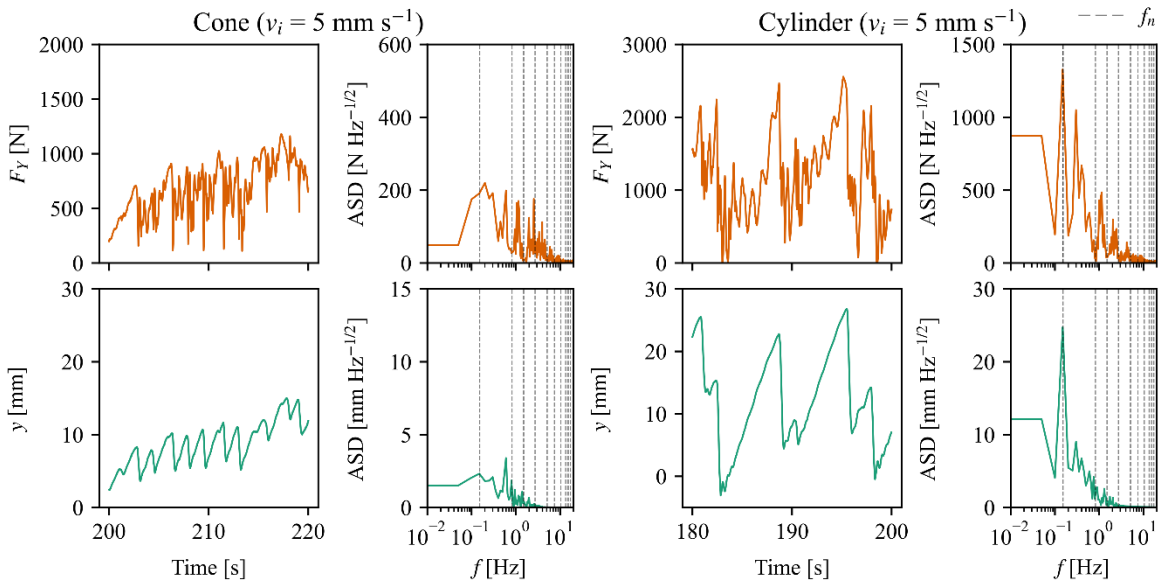

Figure 2. Force (F_Y) and displacement (y) on the cone (left) and on the cylinder (right) at an ice drift speed v_i = 5 mm s^{-1}.

Medium ice drift speed (30 mm s^{-1})

Figure 3 presents the force-time and displacement-time signals and their corresponding ASDs at a medium ice drift speed (v_i = 30 mm s^{-1}). The force-time signal on the cone is characteristic of repeated bending failure. The force increases to a peak, at which the ice fails through bending failure. The cone is then unloaded until the ice edge meets the cone again. The loading period is noisy because the ice fails locally against the cone before bending failure can occur. The force ASD identified the bending failure frequency as slightly higher than the first natural frequency. The bending failure length, estimated as the distance between two upward slopes of a force signal associated with bending failure, varied between 0.07 m and 0.39 m and had a mean of 0.21 m.

The displacement-time signal shows large oscillations that are momentarily in phase with the force oscillations. The displacement ASD indicates that the cone is oscillating at its first natural frequency, with almost negligible contributions from higher-mode frequencies. The momentary synchronization of the force and displacement signals indicates bending failure lock-in at the first natural frequency. Note that the displacement signal becomes negative when the cone is unloaded.

The force-time and displacement-time signals on the cylinder have frequency lock-in characteristics at the second natural frequency. The displacement ASD has a prominent peak at the second natural frequency and a smaller one at the third natural frequency. The displacement oscillations are centered around an offset displacement because the cylinder is always loaded. Moreover, the amplitude of the displacement oscillations is smaller on the cylinder than on the cone.

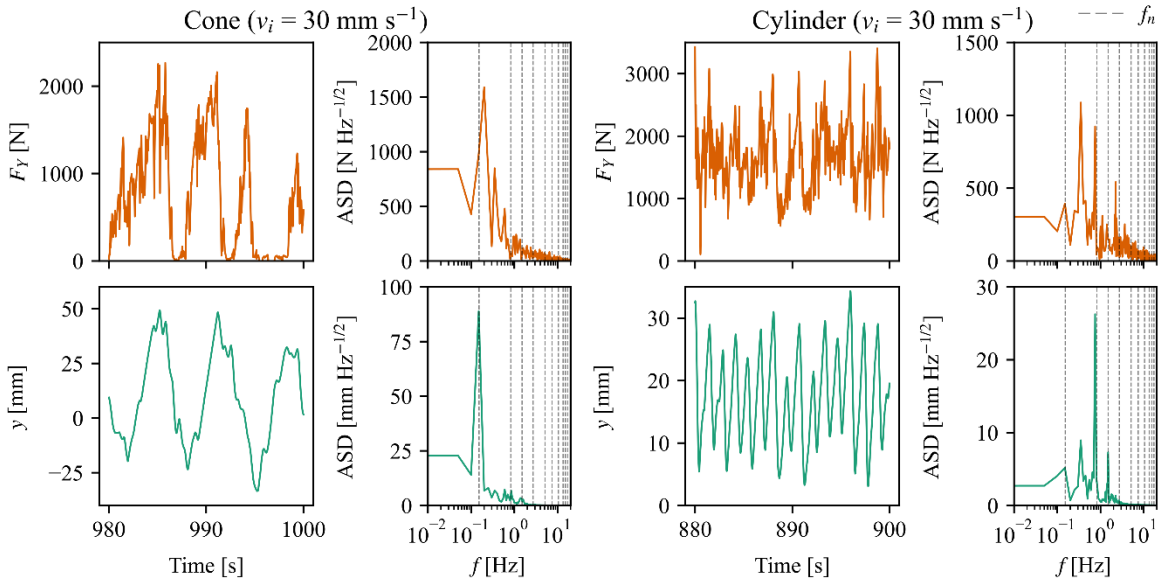

Figure 3. Force (F_Y) and displacement (y) on the cone (left) and on the cylinder (right) at v_i = 30 mm s^{-1}.

High ice drift speed (70 mm s^{-1})

Figure 4 presents the force-time and displacement-time signals and their corresponding ASDs at a high ice drift speed (v_i = 70 mm s^{-1}). The force-time and displacement-time signals on the cone can be divided into two segments at time t = 1290 s. During the first 5 s, the force and displacement signals are composed of a mean superimposed by fluctuations. The force fluctuations are stochastic, while the displacement fluctuations are periodic. The remaining force-time signal is characteristic of repeated bending failure. The corresponding displacement signal shows large oscillations that are momentarily in phase with the force signal. The displacement amplitudes are negative when the cone is unloaded.

The force ASD shows that the bending failure frequency is located between the first and the second natural frequency. The bending failure length varied between 0.06 m and 0.29 m with an outlier at 0.64 m and had a mean of 0.18 m. When the force and displacement oscillations are in phase, the cone oscillates at the second natural frequency, indicating momentary bending failure lock-in at the second natural frequency. Lastly, the displacement ASD also shows oscillations at the first and third natural frequency.

The force-time and displacement-time signals of the cylinder are characteristic of continuous brittle crushing. The force-time signal is composed of stochastic fluctuations around a mean load. The displacement-time signal shows sinusoidal oscillations around a mean displacement. Higher-frequency oscillations superimpose these oscillations. The displacement ASD has a pronounced peak at the first natural frequency and smaller peaks at the second and third natural frequency. Essentially, the cylinder experiences free vibrations while it is loaded with a mean force. Similar force and displacement signals are observed on the cone before t = 1290 s.

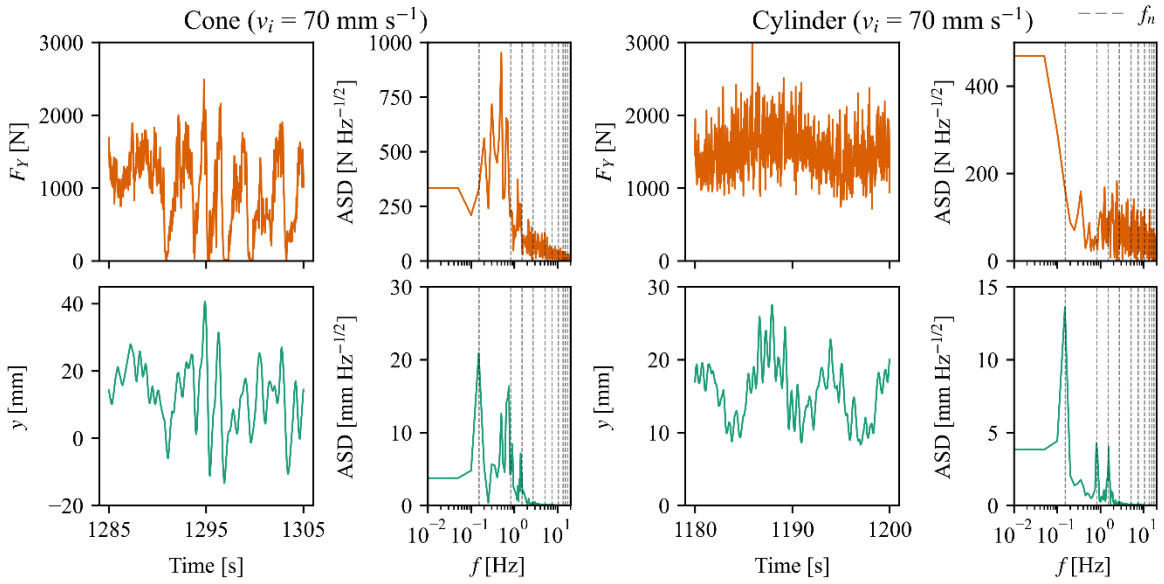

Figure 4. Force (F_Y) and displacement (y) on the cone (left) and on the cylinder (right) at v_i = 70 mm s^{-1}.

DISCUSSION

A final comparison between the cone and the cylinder can be made based on the structural velocity. Figure 5 shows the distribution of the structural velocity of the cone and the cylinder. The data points were limited to the second half of each test to exclude possible peak velocities caused by initial conditions (a test refers to the entire test data at a certain ice drift speed, not only the data shown in Figures 2 to 4). The peak structural velocity ($\dot{y}_{peak}$) is defined as its 99th percentile (Hammer, Willems and Hendrikse, 2023). Figure 5 also shows the domain of peak structural velocities in which lock-in conditions can be expected, according to Toyama et al. (1983). This domain is defined by a linear relationship between the peak structural velocity and the ice drift speed (v_i),

$$\dot{y}_{peak} = \beta v_i, \tag{1}$$

where β is a constant with a value between 1.0 and 1.5.

The distributions of structural velocities clearly show that the cone and cylinder responded differently to the drifting level ice. The differences are more pronounced at medium and high ice drift speeds. At medium ice drift speed, the cone experienced higher structural velocities. This difference is likely due to the cone being periodically unloaded after bending failure events. This unloading allows the cone to accelerate over a larger distance before it makes contact with the ice edge, resulting in higher peak velocities. At high ice drift speed, the cylinder experienced free vibrations, resulting in a symmetrically distributed structural velocity of around 0 mm s^{-1}. The distribution of the structural velocity of the cone is skewed towards positive velocities, indicating forced vibrations.

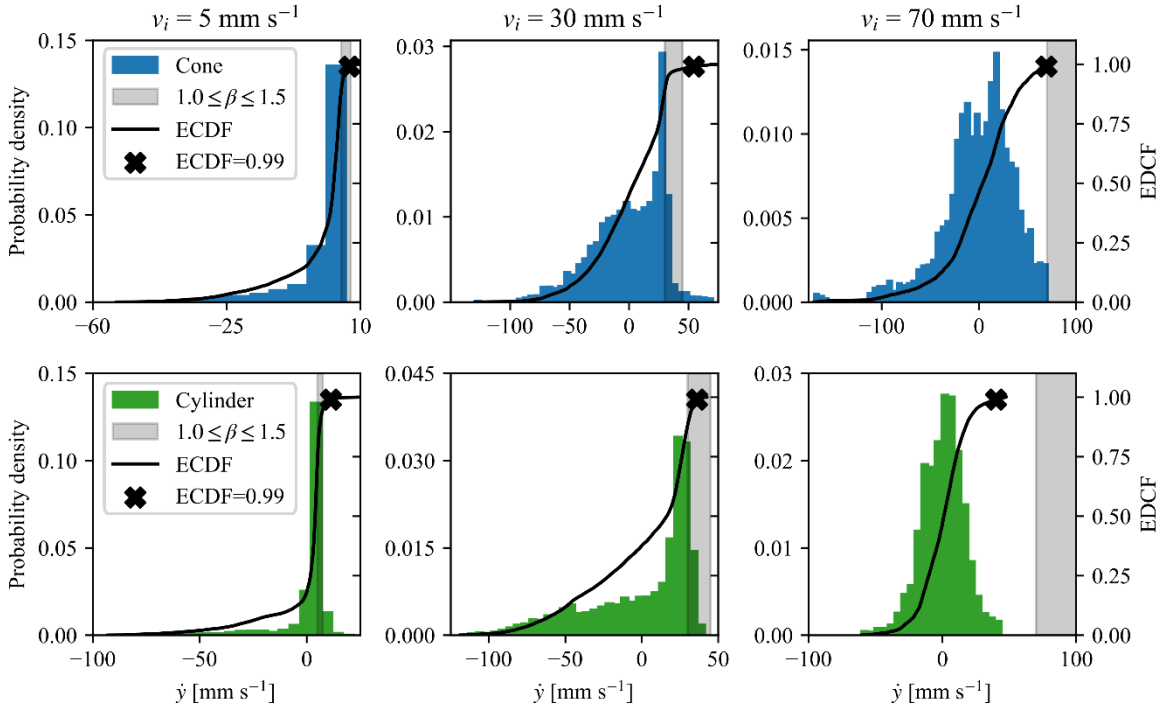

Figure 5. Histograms and empirical cumulative density functions (ECDF) of the structural velocity ($\dot{y}$) for each ice drift speed.

Finally, the peak structural velocity of the cylinder at medium ice drift speed falls within the ice drift range where lock-in is expected according to Equation 1. This was also confirmed with the force-time and displacement-time signals. However, the peak structural velocities of the cone at low and high ice drift speeds also fall into these categories. This suggests that Equation 1 holds for the cylinder but does not hold for the cone.

The aim of the wider test campaign was to explore the use of a HiTL test setup to study ice-structure interaction with compliant conical structures. The structural vibrations associated with local failure at the ice-cone interface at low ice drift speed were unexpected. While the current experiments do not provide enough information to identify the local failure mode with certainty, inspection of the force-time signals and observations made during the tests suggest that the ice failed through a combination of crushing and shear failure. Petry et al. (2024) discusses this failure mode more thoroughly.

The model ice used in this test campaign resulted in more representative bending failure, as the ice wedges did not fail a second time as in previous experiments (Huang, Song, and Shi, 2006; Tian and Huang, 2013; Huang, Ma, and Tian, 2013; Huang, Mu, and Tian, 2013). Modelling bending failure, especially the bending failure length, is essential to study ice-induced vibrations with conical structures as bending failure lock-in occurs at characteristic ice drift speeds where the bending failure frequency matches a natural frequency of the structure. Moreover, this model ice has a similar transition velocity as sea ice, displays a velocity effect, and models crushing failure well (Hammer, Puolakka and Hendrikse, 2024). Nonetheless, full-scale observations of repeated bending failure on a conical structure without rubble formation is needed to understand how the observed local failure and bending failure processes compare to sea ice.

Developing model ice which models all aspects of the different ice failure processes involved in ice-structure interaction is essential to performing model-scale experiments focused on ice-induced vibrations. The numerical structure model used during the experiments was representative of an OWT in the Southern Baltic Sea. However, the results of the conical structure should not be scaled up to full-scale, because the scaling factor was not chosen with respect to a prototype structure, but merely to achieve dynamic ice-structure interaction at reduced-scale. Future experiments with compliant conical structures should explore ways to maintain both representative ice failure modes and load levels through modifying the mechanical properties of the current model ice or investigating and leveraging the relationships between different aspects of conical structures and how they affect ice failure.

CONCLUSIONS

The conical structure experienced four different types of ice-induced vibrations: intermittent brittle crushing and local failure-induced vibrations at a low ice drift speed, bending failure lock-in at medium and high ice drift speeds, and continuous brittle crushing at a high ice drift speed.

- Bending failure lock-in was determined as large amplitude sawtooth waves followed by a period of unloading in the force-time signal and large sinusoidal oscillations in the displacement-time signal. The displacement oscillations were momentarily in phase with the force oscillations.
- Local failure-induced vibrations were determined as low amplitude sawtooth waves and an increasing mean in both the force-time and displacement-time signals. Local failure was determined as combined shear failure and crushing failure of the ice edge. The conical structure moved against the ice-drift direction at each failure event, which resulted in sawtooth waves in the displacement signal.
- Intermittent brittle crushing and continuous brittle crushing had similar force-time and displacement-time characteristics on the conical and the cylindrical structure.

Finally, a comparison of the structural velocities of the conical and the cylindrical structures showed that the lock-in indicator by Toyama et al. (1983) should not be applied to the tested conical structure.

The presented results were part of a wider study into ice-structure interaction with a compliant conical structure. Additional results, focused on a comparison of ice failure against a rigid and a compliant ice cone are presented in Petry et al. (2024).

ACKNOWLEDGEMENTS

Funding from the European Union–NextGenerationEU instrument through Research Council of Finland under grant number (348586) *WindySea – Modelling engine to design, assess environmental impacts, and operate wind farms for ice-covered waters* is acknowledged.

The authors would like to thank Hayo Hendrikse, Tim C. Hammer, Laura van Dijke, Cody C. Owen, Kees van Beek and Jeroen Koning from Delft University of Technology, Jeffrey Hoek and Tom Willems from Siemens Gamesa Renewable Energy, and Teemu Päivärinta and Lasse Turja from Aalto Ice and Wave Tank for their help and assistance before, during, and after the test campaign.

REFERENCES

Barker, A., Timco, G.W., Gravesen, H. and Vølund, P. (2005). 'Ice loading on Danish wind turbines: Part 1: Dynamic model tests', *Cold Regions Science and Technology*, 41(1), pp.1–23.

Brown, T.G., and Määttänen, M. (2009). 'Comparison of Kemi-I and Confederation Bridge cone ice load measurement results', *Cold Regions Science and Technology*, 55, pp.3–13.

Hammer, T.C., Willems, T., and Hendrikse, H. (2023). 'Dynamic ice loads for offshore wind support structure design', *Marine Structures*, 87, p. 103335.

Hammer, T.C. (2024). '*Ice-induced vibrations of offshore wind turbines: an exploration of scaling, hybrid testing, and numerical simulations*', Ph.D. thesis, Delft University of Technology.

Hammer, T.C., and Hendrikse, H. (2024). 'Hardware-in-the-Loop experiments in model ice for analysis of ice-induced vibrations of offshore structures', *Scientific Reports*, 14(1), p.18327.

Hammer, T.C., Puolakka, O., and Hendrikse, H. (2024). 'Scaling ice-induced vibrations by combining replica modeling and preservation of kinematics', *Cold Regions Science and Technology*, 220, pp.104127.

Huang, Y., Song, A., and Shi, Q. (2006). 'The study of ice induced vibration on a compliant cone', In: *Proceedings of the 18th International Conference on Port and Ocean Engineering Under Arctic Conditions (POAC),* Vol. 3, Potsdam, NY, USA, June, pp.1217–1228.

Huang, Y., Ma, J., and Tian, Y. (2013a). 'Model tests of four-legged jacket platforms in ice: Part 1. Model tests and results', Cold Regions Science and Technology, 95, pp.74–85.

Huang, Y., Mu, Y., and Tian, Y. (2013b). 'Model tests of four-legged jacket platforms in ice: Part 2. Analyses and discussions', Cold Regions Science and Technology, 95, pp.86–101.

Li, Z. and Riska, K. (1996). *Preliminary study of physical and mechanical properties of model ice*, Espoo, Finland: Helsinki University of Technology (TKK).

Kärnä, T. And Jochmann, P. (2003). 'Field observations on ice failure modes', In: *Proceedings of the 17th International Conference on Port and Ocean Engineering under Arctic Conditions (POAC)*, Trondheim, Norway.

Petry, A., Puolakka, O., Hammer, T.C., Hendrikse, H., and Polojärvi, A. (2024). *Unexpected ice-induced vibrations on a conical structure in model scale.* Manuscript submitted for publication.

Tian, Y. and Huang, Y. (2013). 'The dynamic ice loads on conical structures', *Ocean Engineering*, 59, pp.37–46.

Toyama, T., Sensu, T., Minami, M., and Yashima, N. (1983). 'Model tests on ice-induced self-excited vibration of cylindrical structures', In: *Proceedings of the 7th International Conference on Port and Ocean Engineering under Arctic Conditions (POAC)*, Vol. 2, Helsinki, Finland, April, pp.834-844.

van der Stap, F.L., Nielsen, M.B., Owen, C.C., van der Male, P., and Hendrikse, H. (2023). 'On the feasibility of monopile foundations for offshore wind in the Baltic Sea', In: *Proceedings of the 27th International Conference on Port and Ocean Engineering under Arctic Conditions (POAC)*, Glasgow, United Kingdom, June.

Xu, N., Yue, Q., Qu, Y., Bi, X. and Palmer, A. (2011). 'Results of Field Monitoring on Ice Actions on Conical Structures', *Journal of Offshore Mechanics and Arctic Engineering*, 133(4), pp.041502.

Xu, N., Yue, Q., Bi, X., Kärnä, T., and Zhang, D. (2015). 'Experimental study of dynamic conical ice force', *Cold Regions Science and Technology*, 120, pp.21–29.

Yue, Q., and Bi, X. (1998). 'Full-scale tests and analysis of dynamic interaction between ice sheet and conical structures', In: *Proceedings of 14th IAHR International Symposium on Ice*, Vol. 2, Potsdam, NY, USA, July, pp.939–945.

Yue, Q., and Bi, X. (2000). 'Ice-induced jacket structure vibrations in Bohai sea', *Journal of Cold Regions Engineering*, 14(2), pp.81–92, 2000.

Ziemer, G., Evers, K.-U., and Voosen, C. (2015). 'Influence of Structural Compliance and Slope Angle on Ice Loads and Dynamic Response of Conical Structures', In: *Proceedings of the ASME 2015 34th International Conference on Ocean, Offshore and Arctic Engineering*, Volume 8: Ian Jordaan Honoring Symposium on Ice Engineering, St. John's, Newfoundland, Canada, May, pp.V008T07A037.